Efficient Bulk Heterojunction Solar Cells Based on a Broadly Absorbing Phenylenevinylene Copolymer Containing Thiophene and Pyrrole Rings

ARTICLE *in* THE JOURNAL OF PHYSICAL CHEMISTRY C · APRIL 2011

Impact Factor: 4.77 · DOI: 10.1021/jp112320b

THE JOURNAL OF PHYSICAL CHEMISTRY C

ARTICLE

pubs.acs.org/JPCC

Efficient Bulk Heterojunction Solar Cells Based on a Broadly Absorbing Phenylenevinylene Copolymer Containing Thiophene and Pyrrole Rings

J. A. Mikroyannidis,*[,†] A. N. Kabanakis,[†] P. Suresh,[‡,§] and G. D. Sharma*[,‡,∥]

[†]Chemical Technology Laboratory, Department of Chemistry, University of Patras, GR-26500 Patras, Greece

[‡]Molecular Electronic and Optoelectronic Device Laboratory, Physics Department, JNV University, Jodhpur, Rajasthan 342005, India

[∥]R & D Center for Science and Engineering, Jaipur Engineering College, Kukas, Jaipur, Rajasthan, India

ABSTRACT: A novel low band gap alternating phenylenevinylene copolymer, **P**, containing thiophene and pyrrole rings was synthesized by Heck polycondensation. It was soluble in common organic solvents and showed a long-wavelength absorption maximum at 596−635 nm and an optical band gap of 1.65 eV. The electrochemical properties and electronic energy levels of **P** were studied by cyclic voltammetry. The highest occupied molecular orbital (HOMO) level of **P** is deeper than that of poly(3-hexylthiophene) (P3HT). The polymer solar cells (PSCs) based on **P** with a modified 1-(3-methoxycarbonyl)-propyl-1-phenyl-[6,6]-C-61 (PCBM) (i.e., **F**) as an electron acceptor shows higher open circuit voltage (V_{oc}) than that for the device based on P3HT. The power conversion efficiency (PCE) for the devices **P**−**F** and **P**−PCBM processed from tetrahydrofuran (THF) solvent is approximately 2.42% and 1.50%, respectively. The enhanced PCE is attributed to the higher value of both V_{oc} and short circuit current (J_{sc}). The PCE of the devices based on **P**−**F** processed from mixed solvents has been further improved. The **P**−**F** blend film cast from mixed solvents shows higher absorption and incident photons to current efficiency (IPCE) with respect to the THF-cast film. The overall PCE for the PSC processed from 1-chloronaphthalene (CN)/THF (thermally annealed) is 4.14%. The improved PCE has been attributed to the increased crystallite size and hole mobility in the blend, resulting in balanced charge transport.

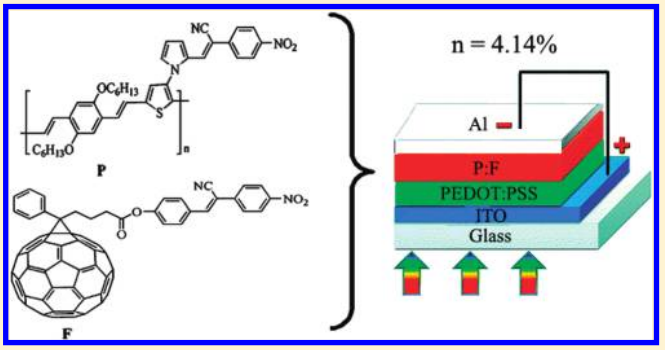

INTRODUCTION

Polymer solar cells have attracted a great deal of attention because of the low-cost, lightweight, and mechanical flexibility.[1−4] Certain articles concerning the manufacture, product integration and application of organic photovoltaic (OPV) devices have been recently reported.[5] Bulk heterojunction (BHJ) polymer solar cells (PSCs) have been emerging as one of the attractive renewable energy sources for the possibility of chemically manipulating the material properties of the polymers combined with easy and cheap processing techniques.[6] In typical BHJ PSCs, conjugated polymers and fullerene derivatives, for example, 1-(3-methoxycarbonyl)-propyl-1-phenyl-[6,6]-C-61 (PCBM) (Scheme 1), function as the light-absorbing/electron-donating and electron-accepting materials, respectively.[7] Therefore, the energy gap and film absorption coefficient of conjugated polymers are two of the most important parameters to be optimized for efficient harvesting of the solar energy and hence realizing high-performance PSCs. The solar spectrum covers a very broad wavelength from ultraviolet to near-infrared (NIR) regions. Theoretically, the ideal band gap of conjugated polymers for PSCs should be around 1.5 eV.[8] However, most conjugated polymers reported so far, such as polythiophenes (PThs) and poly(phenylene vinylene)s (PPVs),[9,10] exhibit optical band gaps larger than or around 2.0 eV and therefore can harvest only visible light. This mismatch of the absorption to the solar spectrum significantly limits the device performance of PSCs. Therefore, development of NIR-absorbing or low band gap polymers is very important. To construct polymers consisting of alternating electron-rich and electron-deficient aromatic units is the most successful strategy to lower the optical band gap of the conjugated polymers.[11] Various electron-deficient units, such as electron-deficient heterocycles,[12,13] perylene diimides,[14] and cyanovinylenes,[15] and several electron-rich units, such as thiophene, pyrrole, fluorene, and carbazole, have been used to construct low band gap polymers. However, of those with NIR absorption,[12d,e,i,16] only a few exhibit power conversion efficiency (PCE) beyond 1%.[12e,16e,16f]

During the past two years, several important low band gap polymers with enhanced absorption abilities appeared and researchers made a breakthrough in fabricating PSC devices with PCEs up to 5−7% based on these polymers.[17] To date, the PCEs

Received: December 28, 2010
Revised: February 22, 2011
Published: March 10, 2011

dx.doi.org/10.1021/jp112320b | J. Phys. Chem. C 2011, 115, 7056–7066

Scheme 1. Chemical Structures of F and PCBM, Which Were Used as Electron Acceptors for the BHJ Solar Cells

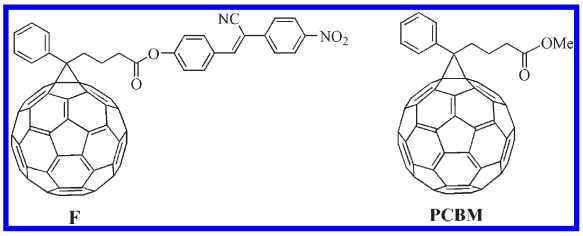

based on conjugated polymer solar cells have reached high up to 8.13% by Solarmer.[18a] A PCE of 8.3% has been reported by Konarka for OPV, which is the current world record.[18b] The polymer plays the key roles of absorbing light, creating excitons for subsequent charge separation, and transporting holes to the anode. It has been realized that an ideal conjugated polymer donor in PSCs should exhibit broad absorption with high absorption coefficient in the visible region, high hole mobility, suitable energy level matching with fullerene acceptor, and appropriate compatibility with fullerene acceptor to form nanoscale bicontinuous interpenetrating network.

Pyrrole-based oligomers have been less intensively studied for organic device applications relative to their oligothienyl homologues.[19,20] This fact may be due, in part, to the limited synthetic routes available to oligopyrroles.[21] A literature survey revealed that certain copolymers containing thiophene and pyrrole rings have been recently synthesized and used as donors for BHJ solar cells. The PCE of these devices ranged from 0.18% to 2.80%.[22−28]

Recently, we have synthesized two low band gap soluble phenylenevinylene copolymers with cyanovinylene 4-nitrophenyl segments. They have been used as electron donors with PCBM as acceptor for BHJ solar cells of PCE up to 4.06%.[29] Moreover, we have very recently synthesized a modified PCBM derivative **F** (Scheme 1), which contains cyanovinylene 4-nitrophenyl segments.[30] It was more soluble than PCBM in common organic solvents due to the increase of the organic moiety. Both solutions and thin films of **F** showed stronger absorption than PCBM in the range of 250−900 nm. BHJ solar cells based on P3HT as electron donor with **F** as electron acceptor displayed a PCE of 4.23%, while the device based on P3HT−PCBM displayed a PCE of 2.93% under the same conditions.[30]

The present investigation describes the synthesis and characterization of a novel low band gap phenylenevinylene copolymer, **P**, which contains thiophene and pyrrole rings. In particular, it carries alternative phenylenevinylene and thiophene along the backbone and a pyrrole side group. The latter is attached to the thiophene ring through the nitrogen and carries cyanovinylene 4-nitrophenyl substituents to broaden the absorption spectrum. The two hexyloxy chains act as solubilizing groups. The dihexyloxyphenylene, thiophene, and pyrrole groups behave as electron donors, while the cyanovinylene 4-nitrophenyl group behaves as an electron-withdrawing moiety. The band gaps estimated from optical absorption and cyclic voltammetry measurements are 1.65 and 1.70 eV, respectively. We have fabricated PSCs with the BHJ active layer (**P**−PCBM and **P**−**F**) deposited from tetrahydrofuran (THF) solvent. We have achieved PCE for the BHJ devices based on **P**−PCBM and **P**−**F** of ∼1.50% and 2.42%, respectively. We have also fabricated PSCs with the BHJ active layer (**P**−**F**) processed from different solvents [1,2-dichlorobenzene (DCB)/THF, 1-chloronaphthalene (CN)/THF] and achieved PCE of 3.16% and 3.66%, respectively. The PSC based on the **P**−**F** blend cast from CN/THF and subsequently thermally annealed shows a PCE of 4.14%. The higher PCE for the devices cast from mixed solvents and further improvement with thermal annealing has been attributed to the increase in the crystallite size of **P**, which facilitates charge transport in the device.

EXPERIMENTAL SECTION

Reagents and Solvents. Nitrobenzyl cyanide was synthesized from the nitration of benzyl cyanide with concentrated nitric and sulfuric acid.[31] It was recrystallized from ethanol. *N*,*N*-Dimethylformamide (DMF) and tetrahydrofuran (THF) were dried by distillation over CaH_2. All other reagents and solvents were commercially purchased and were used as supplied.

Preparation of Compounds and Copolymers. *Compound* ***1***. This compound was synthesized by bromination of thiophene in THF by use of *N*-bromosuccinimide (NBS).[32]

Compound ***2***. 2,5-Dibromothiophene (**1**) (7.10 g, 29.35 mmol) was added dropwise at 0 °C to a stirred mixture of concentrated H_2SO_4 (15 mL) and concentrated HNO_3 (6 mL). Stirring of the mixture at this temperature was continued for 15 min. It was subsequently poured into ice−water and extracted with dichloromethane. The organic layer was dried (Na_2SO_4) and concentrated to afford **2** (6.74 g, 80%). Fourier transform infrared (FT-IR) (KBr, cm^{-1}): 1530, 1336 (nitro), 1504 (aromatic). ^1H NMR ($CDCl_3$) ppm: 7.52 (s, H4 of thiophene). Anal. Calcd for $C_4HBr_2NO_2S$: C, 16.74; H, 0.35; N, 4.88. Found: C, 16.43; H, 0.32; N, 4.62.

Compound ***3***. A slurry of **2** (2.00 g, 6.97 mmol) and fine iron powder (1.50 g, 26.85 mmo) in acetic acid (20 mL) was stirred for 4 h at 80 °C. The reaction mixture was cooled to room temperature, precipitated in 5% aqueous NaOH, and extracted three times with dichloromethane. The combined organic layers were washed with brine and dried with Na_2SO_4, and the solvent was removed under reduced pressure to afford **3** (0.82 g, 46%). FT-IR (KBr, cm^{-1}): 3094 (N−H stretching), 1650 (N−H deformation), 1504 (aromatic). ^1H NMR ($CDCl_3$) ppm: 7.16 (br, 2H, NH_2); 6.64 (s, 1H, H4 of thiophene). Anal. Calcd for $C_4H_3Br_2NS$: C, 18.70; H, 1.18; N, 5.45. Found: C, 18.35; H, 1.07; N, 5.36.

Compound ***4***. A mixture of **3** (0.82 g, 3.18 mmol), 2,5-dimethoxytetrahydrofuran (0.42 g, 3.18 mmol), and glacial acetic acid (15 mL) was stirred and refluxed for 3 h under N_2. It was subsequently concentrated under reduced pressure. Water was added to the concentrate and the mixture was extracted with dichloromethane. The organic layer was dried (Na_2SO_4) and rotary-evaporated to afford **4** (0.73 g, 75%). FT-IR (KBr, cm^{-1}): 1504 (aromatic). ^1H NMR ($CDCl_3$) ppm: 6.70 (m, 1H, H4 of thiophene and 2H, H2, H5 of pyrrole), 6.20 (m, 2H, H3, H4 of pyrrole). Anal. Calcd for $C_8H_5Br_2NS$: C, 31.30; H, 1.64; N, 4.56. Found: C, 30.95; H, 1.77; N, 4.63.

Compound ***5***. A flask was charged with a solution of **4** (0.98 g, 3.18 mmol) in 1,2-dichloroethane (30 mL). DMF (0.26 g, 3.50 mmol) and $POCl_3$ (0.54 g, 3.50 mmol) were added dropwise, and the mixture was refluxed for 17 h. After this was cooled to room temperature, a saturated aqueous solution of CH_3COONa (30 mL) was added and the mixture was refluxed for 20 min. The organic layer was then washed with water and dried over Na_2SO_4. Solvent

removal and column chromatography (silica gel/dichloromethane) gave **5** (0.36 g, 34%). FT-IR (KBr, cm^{-1}): 1667 (carbonyl), 1504 (aromatic). ^1H NMR ($CDCl_3$) ppm: 9.50 (s, 1H, formyl), 7.12−7.01 (m, 2H, H3, H5 of pyrrole), 6.70 (m, 1H, H4 of thiophene), 6.34 (m, 1H, H4 of pyrrole). Anal. Calcd for $C_9H_5Br_2NOS$: C, 32.27; H, 1.50; N, 4.18. Found: C, 32.03; H, 1.36; N, 4.10.

Compound ***6***. This compound was prepared by Stille coupling reaction[33] of 1,4-dibromo-2,5-bis(hexyloxy)benzene with tributylvinyltin.[34]

Copolymer ***7***. A flask was charged with a mixture of **5** (0.3649 g, 1.09 mmol), **6** (0.3600 g, 1.09 mmol), $Pd(OAc)_2$ (0.0102 g, 0.045 mmol), P(*o*-tolyl)$_3$ (0.0762 g, 0.250 mmol), DMF (7 mL), and triethylamine (3 mL). The mixture was heated at 90 °C for 24 h under N_2. Then it was filtered and the filtrate was poured into methanol to afford **7**. The crude product was purified by dissolving in THF and precipitating into methanol (0.4059 g, 74%). FT-IR (KBr, cm^{-1}): 2952, 2928 (C−H stretching of hexyloxy), 1667 (carbonyl), 1210 (ether bond), 1504 (aromatic). ^1H NMR ($CDCl_3$) ppm: 9.50 (s, 1H, formyl), 7.12−7.01 (m, 2H, H3, H5 of pyrrole and 4H, vinylene), 6.75−6.70 (m, 1H, H4 of thiophene and 2H, phenylene ortho to oxygen), 6.34 (m, 1H, H4 of pyrrole), 3.96 [m, 4H, $OCH_2(CH_2)_4CH_3$], 1.81 [m, 4H, OCH_2CH_2-$(CH_2)_3CH_3$], 1.37 [m, 12H, $O(CH_2)_2(CH_2)_3CH_3$], 0.91 [t, 6H, $O(CH_2)_5CH_3$]. Anal. Calcd for $(C_{31}H_{37}NO_3S)_n$: C, 73.92; H, 7.40; N, 2.78. Found: C, 73.34; H, 7.56; N, 2.89.

Copolymer ***P***. A flask was charged with a solution of **7** (0.6732 g, 1.337 mmol of the repeating unit) and 4-nitrobenzyl cyanide (0.2168 g, 1.337 mmol) in DMF (15 mL). Sodium hydroxide (0.18 g, 4.50 mmol) dissolved in ethanol (5 mL) was added portionwise to the stirred solution. The mixture was stirred for 1 h at room temperature under N_2 and then was concentrated under reduced pressure. Water was added to the concentrate and **P** precipitated as a green solid. It was filtered, washed thoroughly with water, and dried to afford **P**. The crude product was purified by dissolving in THF and precipitating into methanol (0.63 g, 73%). FT-IR (KBr, cm^{-1}): 2950, 2926 (C−H stretching of hexyloxy), 2174 (cyano), 1522, 1350 (nitro), 1210 (ether bond), 965 (*trans*-vinylene), 1014 (cyanovinylene). ^1H NMR ($CDCl_3$) ppm: 8.18 (m, 2H, phenylene ortho to nitro), 7.72 (s, 1H, cyanovinylene), 7.50 (m, 2H, phenylene meta to nitro), 7.12−7.01 (m, 2H, H3, H5 of pyrrole and 4H, vinylene), 6.75−6.70 (m, 1H, H4 of thiophene and 2H, phenylene ortho to oxygen), 6.34 (m, 1H, H4 of pyrrole), 3.96 [m, 4H, OCH_2-$(CH_2)_4CH_3$], 1.81 [m, 4H, $OCH_2CH_2(CH_2)_3CH_3$], 1.37 [m, 12H, $O(CH_2)_2(CH_2)_3CH_3$], 0.91 [t, 6H, $O(CH_2)_5CH_3$]. Anal. Calcd for $(C_{39}H_{41}N_3O_4S)_n$: C, 77.31; H, 6.38; N, 6.48. Found: C, 76.82; H, 6.24; N, 6.57.

Characterization Methods. IR spectra were recorded on a Perkin-Elmer 16PC FT-IR spectrometer with KBr pellets. ^1H NMR (400 MHz) spectra were obtained on a Bruker spectrometer. Chemical shifts (δ values) are given in parts per million with tetramethylsilane as an internal standard. UV−vis spectra were recorded on a Beckman DU-640 spectrometer with spectrograde THF. Elemental analyses were carried out with a Carlo Erba model EA1108 analyzer. Gel-permeation chromatography (GPC) analysis was conducted with a Waters Breeze 1515 apparatus equipped with a 2410 differential refractometer as a detector (Waters Associate) and Styragel HR columns with polystyrene as a standard and THF as an eluent. The photoluminescence (PL) spectra of the thin films were obtained on a Perkin-Elmer luminescence spectrometer.

Electrochemical cyclic voltammetry was conducted on an EDCH electrochemical instrument in a 0.1 mol/L acetronitrile solution of tetrabutylammonium hexafluorophosphate (Bu_4NPF_6) at a potential scan rate of 100 mV/s with Ag/Ag^+ reference electrode and platinum wire counter electrode. The polymer film was formed by drop-casting 1.0 μL of polymer solution in THF on the working electrode and then drying in air.

Device Fabrication and Characterization. The PSCs were fabricated on precleaned indium tin oxide (ITO) coated glass substrates. A layer of PEDOT−PSS (80 nm) was deposited on ITO coated glass from poly(3,4-ethylenedioxythiophene)−poly (styrenesulfonate) (PEDOT−PSS) aqueous solution at 2000 rpm and the layer was subsequently dried at 100 °C for 20 min in air. A blend of **P** and either PCBM or **F** (1:1 w/w), 10 mg/mL in various solvents, was stirred for 2 h and then spin-coated (1500 rpm for 30 s) on top of the PEDOT−PSS layer. The thickness of the active layer is approximately 90 nm. The device was completed by depositing 80 nm thick layer of aluminum (Al) at pressure of less than 10^{-5} Torr. The active area of the device was 10 mm^2. Device preannealing was carried out at 120 °C for 5 min in ambient conditions by placing it on a hot plate before the deposition of the Al electrode, and then it was cooled to room temperature.

The current−voltage characteristics ($J-V$) were measured on a computer-controlled Keithley electrometer. A xenon lamp coupled with AM 1.5 solar filter was used as the light source and the optical power at the device was around 100 mW/cm^2. The incident photons to current efficiency (IPCE) spectra of the devices were measured with a monochromator and the resulting photocurrent was measured with a Keithley electrometer under short circuit conditions. The devices were tested only in the laboratory under ambient conditions at room temperature.

The hole-only devices, that are ITO/PEDOT−PSS/**P**−**F**/Au, were used to estimate the hole mobility in the blend films and were fabricated as described above except that the top electrode was replaced with Au. Electron-only devices having structure Al/**P**−**F**/Al were also fabricated by spin-coating the active layer on glass/Al substrates, followed by deposition of the Al electrode. The dark $J-V$ characteristics of the devices were measured on an electrometer under ambient conditions.

RESULTS AND DISCUSSION

Synthesis and Characterization. Scheme 2 outlines the seven-step reaction for the synthesis of copolymer **P**. In particular, the bromination of thiophene by *N*-bromosuccinimide (NBS) afforded 2,5-dibromothiophene (**1**).[32] The nitration of the latter using concentrated sulfuric acid and concentrated nitric acid gave the nitro derivative (**2**). Note that the nitration of **1** by means of fuming sulfuric acid and fuming nitric acid yields 2,5-dibromo-3,4-dinitrothiophene.[35] The reduction of **2** using iron powder and glacial acetic acid gave 2,5-dibromo-4-aminothiophene (**3**). Compound **3** reacted with 2,5-dimethoxytetrahydrofuran in glacial acetic acid to afford **4**. The latter was formylated by DMF and $POCl_3$ in 1,2-dichloroethane to give **5**. The Heck polycondensation of **5** with **6** in DMF, using Et_3N as acid scavenger and $Pd(OAc)_2$ as catalyst, gave the alternating copolymer **7**. Finally, **7** reacted with 4-nitrobenzyl cyanide in the presence of NaOH to afford the target copolymer **P**. This reaction aims to broaden the absorption spectrum of **P** due to the formation of the cyanovinylene 4-nitrophenyl segment.[29]

Both copolymers **7** and **P** were soluble in common organic solvents such as THF, chloroform, and dichloromethane owing

Scheme 2. Synthesis of Copolymer P

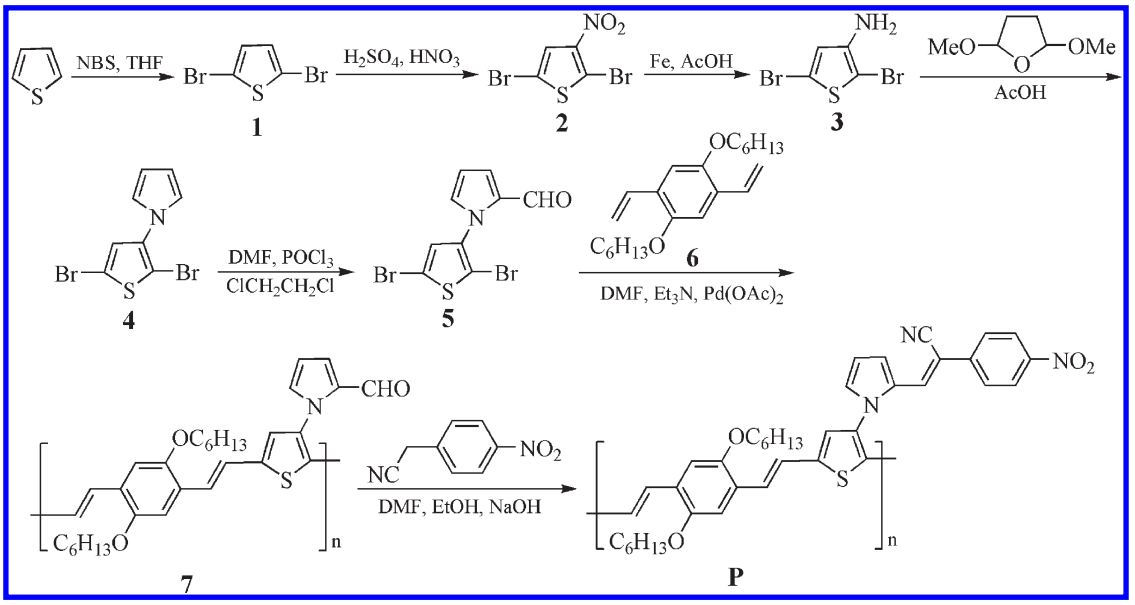

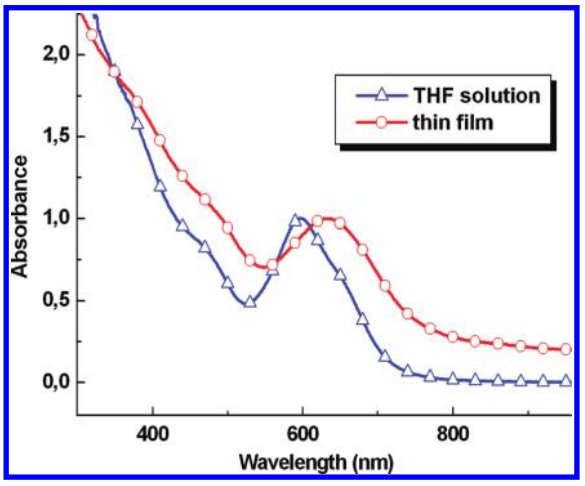

Figure 1. UV−visible spectra of copolymer **P** in THF solution and thin film.

to the hexyloxy side groups. They had number-average molecular weight (M_n) of 12 500 and 13 200 by GPC, with polydispersity of 2.3 and 2.5 for **7** and **P**, respectively.

The intermediate compounds **2**−**5** and copolymers **7** and **P** were characterized by FT-IR and ^{1}H NMR spectroscopy. Copolymer **P** showed characteristic absorption bands at 2950, 2926 (C−H stretching of hexyloxy), 2174 (cyano), 1522, 1350 (nitro), 1210 (ether bond), 965 (*trans*-vinylene), and 1014 cm^{-1} (cyanovinylene). On the other hand, the ^{1}H NMR spectrum of **P** displayed upfield signals at 8.18 (phenylene ortho to nitro), 7.72 (cyanovinylene), and 7.50 ppm (phenylene meta to nitro). The pyrrole, thiophene, vinylene, and phenylene ortho to oxygen resonated at the region of 7.12−6.34 ppm. Finally, the hexyloxy chains resonated at 3.96−0.91 ppm.

Photophysical and Electrochemical Properties. Figure 1 presents the UV−visible absorption spectra of **P** in both dilute (10^{-5} M) THF solution and thin film, while Table 1 summarizes all photophysical properties of this copolymer. The absorption

Table 1. Optical and Electrochemical Properties of Copolymer P

$\lambda_{a,max}$[a] in solution (nm)	596
$\lambda_{a,max}$[a] in thin film (nm)	635
thin film absorption onset (nm)	752
E_g^{opt}[b] (eV)	1.65
E_{onset}^{ox} (V)	0.45
E_{onset}^{red} (V)	−1.3
HOMO (eV)	−5.15
LUMO (eV)	−3.45
E_g^{el}[c] (eV)	1.70

[a] $\lambda_{a,max}$ = absorption maximum from UV−vis spectrum in THF solution or in thin film. [b] E_g^{opt} = optical band gap determined from absorption onset in thin film. [c] E_g^{el} = electrochemical band gap determined from cyclic voltammetry.

curves were broad and extended from 300 nm up to approximately 750 nm for solution and 800 nm for thin film, which is advantageous for photovoltaic (PV) applications. This feature could be attributed to an intramolecular charge transfer (ICT) between the electron-donating (dihexyloxyphenylene, thiophene, pyrrole) and the electron-withdrawing (cyanovinylene 4-nitrophenyl) moieties. The long-wavelength absorption maximum ($\lambda_{a,max}$) was at 596 nm for solution and 635 nm for thin film. The thin film absorption curve of **P** was broader and red-shifted relative to that in solution because of intermolecular interactions in solid state. The absorption band and onset was red-shifted as compared to that for P3HT.[30] The optical band gap (E_g^{opt}) of **P** was calculated from the thin film absorption onset (752 nm) and was 1.65 eV, which is much smaller than that of the widely used regioregular P3HT (1.95 eV).

The highest occupied molecular orbital (HOMO) and the lowest unoccupied molecular orbital (LUMO) energy levels of conjugated polymers are important parameters in the design of optoelectronic devices, and they can be estimated from the onset oxidation and reduction potentials.[36] The onset oxidation

dx.doi.org/10.1021/jp112320b |*J. Phys. Chem. C* 2011, 115, 7056–7066

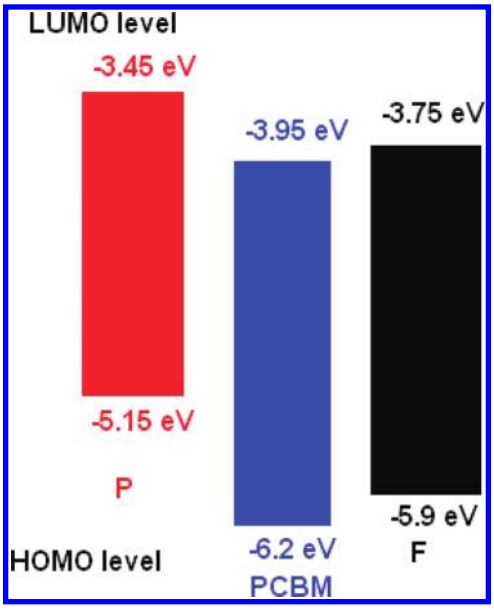

Figure 2. HOMO and LUMO energy levels for **P**, PCBM, and **F**.

potential (E_{onset}^{ox}) and reduction potential (E_{onset}^{red}) for copolymer **P** are 0.45 and −1.3 V versus Ag/Ag^+, respectively. The HOMO and LUMO energy levels are estimated from the following equations:

$$E_{HOMO} = -q(E_{onset}^{ox} + 4.7)\ \text{eV}$$

$$E_{LUMO} = -q(E_{onset}^{red} + 4.7)\ \text{eV}$$

The values of HOMO and LUMO levels are listed in Table 1. The energy levels of **P**, PCBM, and **F** are shown in Figure 2. The HOMO and LUMO energy levels for **P** are −5.15 and −3.45 eV, respectively. The HOMO level of **P** is very close to the threshold HOMO level (−5.2 eV) for a conjugated polymer used as donor in efficient BHJ polymer solar cells[37] and is deeper than that of P3HT. In addition, the deeper HOMO level of a polymer is desirable for higher open circuit voltage (V_{oc}) of PSCs with polymer donor materials, because V_{oc} is usually proportional to the difference between the LUMO level of the acceptor and the HOMO level of the donor.[38] The lower HOMO level of **P** is attributed to the cyanovinylene 4-nitrophenyl acceptor group, which is beneficial for chemical stability in ambient conditions. The electrochemical band gap ($E_g^{el} = E_{LUMO} - E_{HOMO}$) is about 1.70 eV, which is slightly higher than the optical band gap (E_g^{opt}) estimated from the UV−visible absorption onset. This is a common phenomenon in the organic materials due to their higher exciton binding energy.[39] It is generally accepted that an energy difference of 0.3 eV between the LUMO levels of acceptor and donor materials (i.e., LUMO−LUMO offset) used in BHJ is necessary for efficient photoinduced electron transfer from the polymer to acceptor material.[40] The LUMO levels of PCBM and **F** are −3.95 and −3.75 eV, respectively. The LUMO−LUMO offset between **P** and either PCBM or **F** is larger than 0.3 eV, and therefore it is expected that excitons can be easily dissociated at the donor/acceptor (D/A) interfaces formed between **P** and either PCBM or **F**. Furthermore, the HOMO energy level of **P** (−5.15 eV) is well aligned with the HOMO level of PEDOT−PSS (−5.1 eV), indicating that holes can be easily transported from the HOMO level of **P** to PEDOT−PSS. Consequently, copolymer **P** can be used as electron donor, with PCBM or **F** as electron acceptor, for BHJ polymer solar cells.

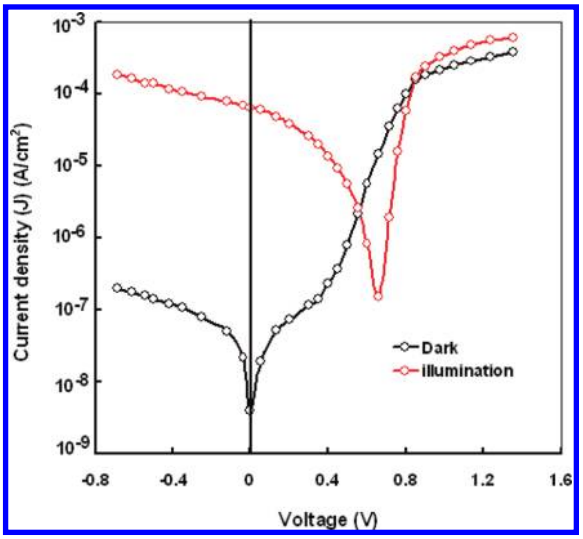

Figure 3. Current−voltage ($J-V$) characteristics of ITO/PEDOT−PSS/**P**/Al device in the dark and under illumination.

Electrical and Photovoltaic Properties of P. We have investigated the current−voltage ($J-V$) characteristics of **P** using a single-layer device having structure ITO/PEDOT−PSS/**P**/Al, in the dark, which are shown in Figure 3. The $J-V$ characteristics of the device in the dark show a rectification effect when positive potential is applied to the ITO/PEDOT−PSS electrode with respect to the Al electrode. Since the HOMO level of **P** is very close to the HOMO level of PEDOT−PSS, this electrode behaves as an Ohmic contact for hole injection from the PEDOT−PSS-coated ITO electrode into the HOMO level of **P**. However, the LUMO level of **P** is very far from the work function of Al (−4.2 eV) and forms a Schottky barrier for electron injection from Al into the LUMO of **P**. Therefore, the rectification effect is due to the formation of a Schottky barrier at the Al/**P** interface.

The charge carrier mobility of conjugated polymers used as photoactive layer in organic PV devices is also an important factor that influences the charge transport in the device, hence the short circuit current (J_{sc}). The hole mobility of **P** was measured by the space charge limited current (SCLC) method, with the device structure ITO/PEDOT−PSS /**P**/Au and the hole mobility is 5.3×10^{-6} $cm^2/(V \cdot s)$, which is similar to other conjugated polymers.

The $J-V$ characteristics of the ITO/PEDOT−PSS/**P**/Al device under illumination are also shown in Figure 3, and the values of J_{sc}, V_{oc}, FF, and PCE are 6.46×10^{-2} mA/cm^2, 0.66 V, 0.38, and 0.016%, respectively. In spite of broader absorption in the visible region and low band gap of **P**, the PCE of the device is very small. This feature is attributed to the fact that all excitons generated in the **P** layer after the absorption of light are not dissociated into free charge carriers because of the short exciton diffusion length in the organic layer. Since the built-in potential present at the Al/**P** interface in the ITO/PEDOT−PSS/**P**/Al device is responsible for the exciton dissociation into free charge carrier, only the photogenerated excitons are able to reach this interface and contribute to the photocurrent. The excitons generated far away from the Al/**P** interface are decayed during their diffusion toward this interface and do not contribute to the photocurrent, thus leading to low fill factor and PCE.

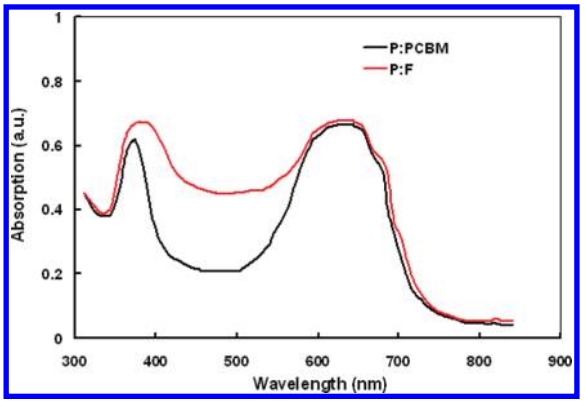

Figure 4. Optical absorption spectra of **P**−PCBM and **P**−**F** blended thin films cast from THF.

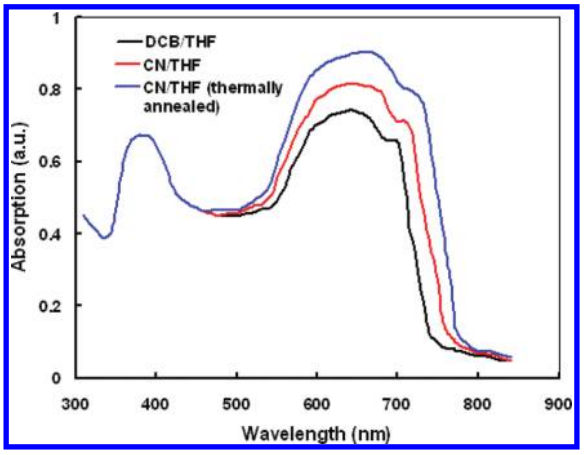

Figure 5. Optical absorption spectra of **P**−**F** blend thin films cast from DCB/THF, CN/THF, and CN/THF (thermally annealed).

Optical Properties of P−PCBM and P−F Blends. Figure 4 shows the UV−visible absorption spectra **P**−PCBM and **P**−**F** thin films cast from THF solvent. The absorption peak in the lower-wavelength region corresponds to either PCBM or **F** in their blends, whereas the peak in the longer-wavelength region corresponds to **P**. Copolymer **P** can harvest photons in the long-wavelength range from 550 to 750 nm. Between 400 and 550 nm, the absorption coefficient of **F** is larger than that of PCBM. In the shorter-wavelength region (below 400 nm), PCBM exhibits the well-known resolved peak. However, for **F**, it is difficult to resolve the peak in the same wavelength region. This indicates that the change of functional group on fullerene induces an increase in absorption in the visible range and affects its electronic structure.[41] The overall absorption spectrum of **P**−**F** is broader from 350 to 750 nm as compared to that of **P**−PCBM. We expect that **P**−**F** can harvest more photons from the whole visible range than the **P**−PCBM blend.

Optical absorption spectra of the **P**−**F** blend cast from mixed solvents (DCB/THF, CN/THF, and thermally annealed CN/THF) are shown in Figure 5. Upon the addition of either DCB or CN into the blend solution in THF, the absorption band is red-shifted and the intensity is also increased. A further red shift in the absorption band has also been observed for the thermally annealed blend. A higher crystallinity degree of **P** was indicated by a red shift in absorption band; a clear vibronic shoulder appeared around 700 nm, which indicates enhanced interchain $\pi-\pi^*$ stacking. The blend film cast from mixed solvents showed higher crystallinity than that cast from THF solvent, which is due to the different vapor pressure and boiling point of the solvents. It can be seen from Figure 5 that the vibronic shoulder in the longer-wavelength region is more distinguishable for the thermally annealed blend film, which indicates that the thermal

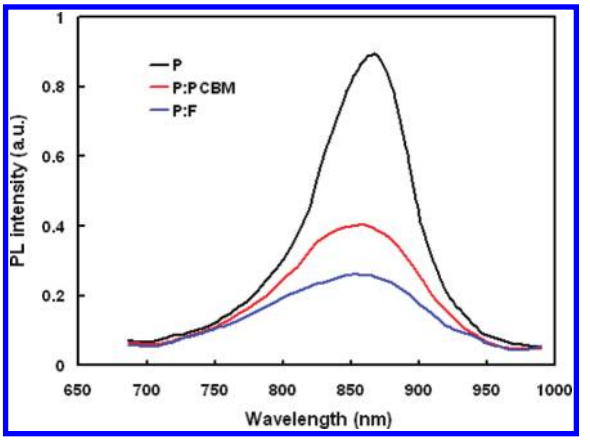

Figure 6. Photoluminescence (PL) spectra of **P**, **P**−PCBM, and **P**−**F** thin films.

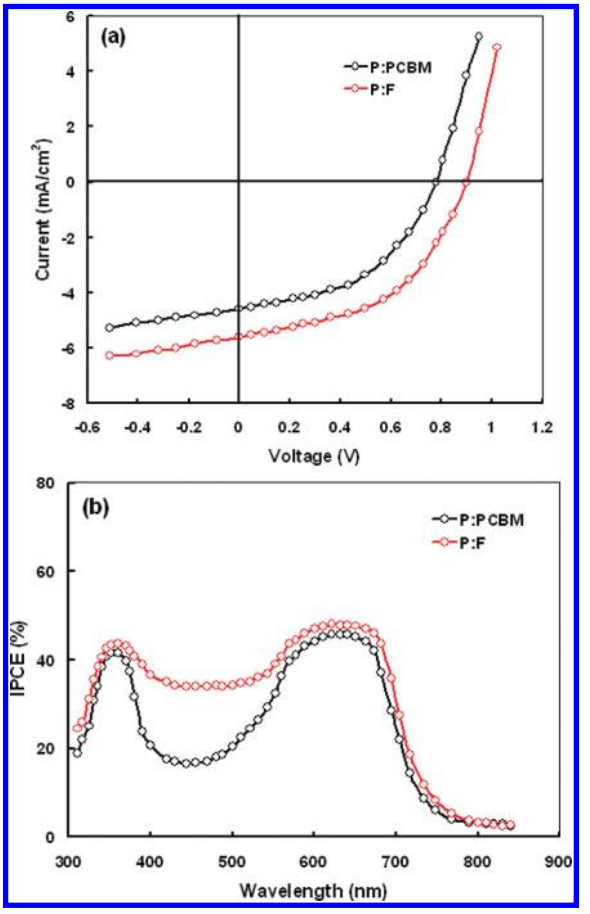

Figure 7. (a) $J-V$ characteristics and (b) IPCE spectra of BHJ devices based on **P**−PCBM and **P**−**F** blends sandwiched between ITO/PEDOT−PSS and Al electrodes.

dx.doi.org/10.1021/jp112320b |*J. Phys. Chem. C* 2011, 115, 7056–7066

Table 2. Photovoltaic Parameters of ITO/PEDOT−PSS/P−(PCBM or F)/Al Devices Cast from Different Solvents

blends	J_{sc} (mA/cm^2)	V_{oc} (V)	FF	PCE (%)
P−PCBM[a]	4.60	0.78	0.42	1.50
P−**F**[a]	5.70	0.90	0.48	2.42
P−**F**[b]	6.50	0.88	0.54	3.16
P−**F**[c]	7.16	0.88	0.57	3.66
P−**F**[d]	8.40	0.86	0.58	4.14

[a] Cast from THF. [b] Cast from DCB/THF. [c] Cast from CN/THF. [d] Cast from CN/THF and thermally annealed.

annealing process further enhanced the crystallinity of the blend. The improved crystallinity of the blend, which is facilitated through self-organized chain stacking, can enhance not only the hole transport but also the light-harvesting capabilities, thus improving the photocurrent in the PV devices.

The photoluminescence (PL) spectra of the pristine **P** film and blended films with PCBM or **F** were also recorded (Figure 6). The wavelength of maximum emission (0.88) for the **P** film is approximately 870 nm, and the emission edge occurs in the region of 950 nm, which is a typical emission spectrum of low band gap polymers. The PL emission is moderately quenched when either PCBM (0.40) or **F** (0.26) is blended with **P**. The PL quenching behavior can be explained by the aggregation-induced self-quenching of the excited polymer states and PCBM or **F** units. The PL quenching might also be a result of intermolecular electron transfer from the photoexcited copolymer to PCBM or **F**. The photoinduced charge transfer in other conjugated molecular composites by PL quenching can be found in the literature and is a prerequisite for efficient organic solar cells. The degree of PL quenching is higher for the **P**−**F** blend as compared to **P**−PCBM, which indicates more efficient photoinduced charge transfer for the **P**−**F** blend.

Photovoltaic Properties of BHJ Devices. Initially, to find the optimum blend ratio, devices with **P**−PCBM blend were prepared and tested with various mixture ratios (1:1, 1:2, and 1:4 w/w) cast from THF solvent. We found that the optimum mixture ratio for the blend is 1:2. Therefore, we have fabricated all devices with BHJ active layer having a mixture ratio of 1:2 (w/w). Figure 7a shows the $J-V$ characteristics under illumination intensity of 100 mW/cm^2 for the devices with **P**−PCBM and **P**−**F** cast from THF solvent. The PV parameters—short circuit current (J_{sc}), open circuit voltage (V_{oc}), fill factor (FF), and power conversion efficiency (PCE)—are summarized in Table 2. The solar cells with **P**−PCBM and **P**−**F** yield PCE values of 1.50% and 2.42%, respectively. The increase in PCE based on **P**−**F** blend is due to the increase in both J_{sc} and V_{oc}. From Table 1 and Figure 2, it can be seen that the difference between the HOMO of **P** and the LUMO of PCBM is around 1.2 eV. For **F**, the LUMO level is ~0.2 eV higher than that of PCBM. Since the most important factor that determines V_{oc} in the BHJ solar cell is the difference between HOMO of the donor and LUMO of the acceptor, we attribute the increase in V_{oc} obtained with **F** to its higher LUMO value. The value of V_{oc} for both devices is higher than that reported for the device based on P3HT as donor, which results from the lower HOMO level of **P** as compared to P3HT.

Figure 7b shows the IPCE measurement for both **P**−PCBM and **P**−**F** solar cells. The overall IPCE spectrum of the **P**−**F**-based device is higher than that of **P**−PCBM, which is in agreement with the J_{sc} obtained from the $J-V$ characteristics.

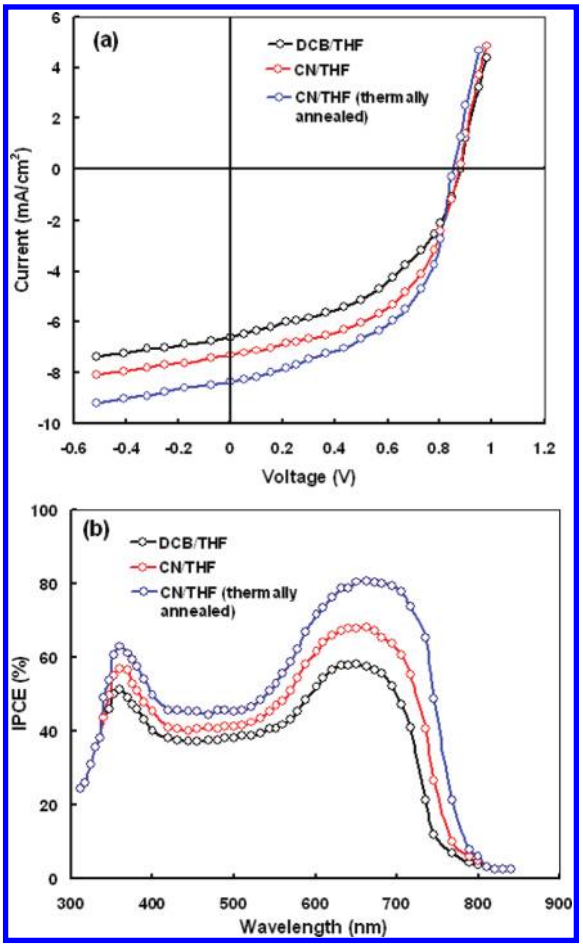

Figure 8. (a) $J-V$ characteristics and (b) IPCE spectra of ITO/PEDOT−PSS/**P**−**F**/Al BHJ devices prepared from different solvents.

When the IPCE spectra of the devices are compared with the absorption spectra of blend films, the photoresponse of the devices is similar to the corresponding absorption spectra of the blend films used for the fabrication of devices. However, the IPCE value in the wavelength region of 350−550 nm for the device based on **P**−**F** is higher than that for the device based on **P**−PCBM, which is consistent with the absorption spectra of **P**−**F** blend. The higher value of IPCE for the device based on **P**−**F** is attributed to the photocurrent contribution due to exciton generation in the **F** component of the **P**−**F** blend and their subsequent dissociation into free charge carriers at the D/A interfaces formed between **P** and **F** in the BHJ active layer. We assume that the increased value of J_{sc} and thereby IPCE is attributed to increased absorption in the wavelength range 350−550 nm, arising from **F**. The replacement of PCBM by the modified PCBM (**F**) shows a wide absorption band at 350−750 nm, which causes an increased PCE of the device. The PCE value of the devices based on **P**−PCBM and **P**−**F** is still low as compared to that for the P3HT−PCBM-based device (2.93%). Since the PL emission is not fully quenched for these blends, we assume that all the excitons generated in the BHJ layer are not fully dissociated into free charge carriers. This might be one of the reasons for the low PCE of these devices.

One particularly effective way to control phase separation in BHJ devices precisely at the time of thin film deposition, and therefore improve the performance, is by processing with solvent

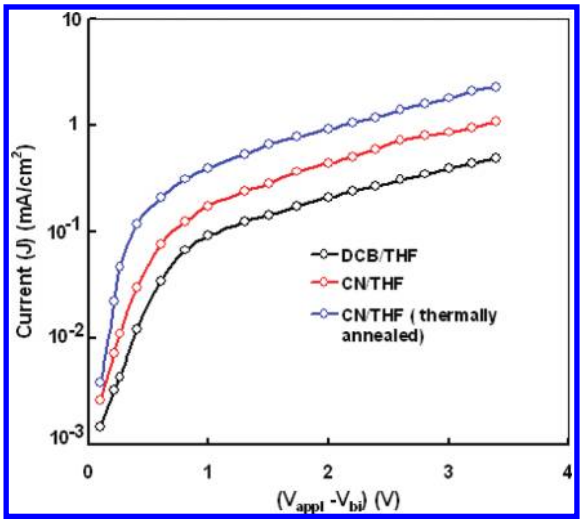

Figure 9. $J-V$ characteristics of ITO/PEDOT−PSS/**P**−**F**/Au hole-only devices prepared from different solvents.

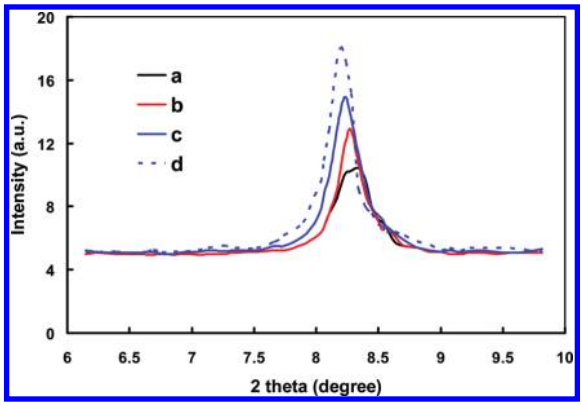

Figure 10. XRD profiles of **P**−**F** blends cast from (a) THF, (b) DCB/THF, (c) CN/THF, and (d) CN/THF (thermally annealed).

additives.[42] Criteria that have emerged for selecting potentially useful additives include the following: (i) it needs to have a higher boiling point than the parent solvent and (ii) it must be a poor solvent for the conjugated polymer and better solvent for the fullerene components. Such a combination of properties leads to aggregation of the polymer in solution, which translates to an increase in the sizes of the BHJ domains in the film. Because the morphologies of the polymer-based active layers were directly influenced by the rates of solvent evaporation of the cast blends, we have investigated the PV response of the device based on **P**−**F** blend cast from mixed solvents (DCB/THF and CN/THF). Since the PCE for the device based on **P**−**F** is higher than that for **P**−PCBM, we have investigated the effect of additives on the PV performance of the BHJ device based on **P**−**F** thin film blend. We have varied the solvent ratios (DCB or CN concentration with respect to THF) from 0 to 2.5 vol % and found that the optimized DCB or CN concentration is 1.75 vol %. Figure 8a displays the measured $J-V$ characteristics of the optimized **P**−**F** PSC devices prepared with additive and with postthermal treatments, under illumination (100 mW/cm^2). The PV parameters estimated from these characteristics are summarized in Table 2. Without thermal treatment, V_{oc} and J_{sc} of the PSCs with CN or DCB additives increased, in comparison to the device without additive (Figure 7a). The PCEs of PSCs with DCB and CN additives increased to 3.16% and 3.66%, respectively.

Thermal annealing is also very important for PSCs with additives. The $J-V$ characteristics of the device based on thermally annealed **P**−**F** blend film cast from CN/DCB solvent are also shown in Figure 8a and the photovoltaic parameters are listed in Table 2. All the PV parameters of the device were improved for the thermally annealed blend. The highest PCE reached 4.14% for the PSC based on **P**−**F** with the additive of CN (thermally annealed). Figure 8b gives the IPCE spectra of PSCs with additives and with thermal treatment. In comparison with the IPCE spectrum of the device without additive, the IPCE values of PSCs without additive increased significantly in the wavelength range of 500−750 nm, which corresponds to absorption of the conjugated copolymer **P**. This indicates that both DCB and CN additives are beneficial to the absorption of **P**. The value of IPCE is 58% and 68% for DCB/THF- and CN/THF-cast devices, respectively. This value has been further improved up to 81% when the device based on CN/THF is thermally annealed.

Since J_{sc} of the PSCs is the result of light absorption, exciton dissociation, and charge transport, these mechanisms are also crucial for the overall PCE. Given that an increase in J_{sc} mainly affected the PCE, the charge transport properties of the devices were studied. The hole and electron mobilities of the **P**−**F** blend film were investigated, by space charge limit current (SCLC) measurements,[43] with electron-only/hole-only devices. Figure 9 shows the dark currents of ITO/PEDOT−PSS/**P**−**F**/Au devices, with corrected bias, which was determined as the difference between the work function of Au and the HOMO level of **P**. In the trap-free region over the trap-filled limit, which is the limit of the presence of carrier traps, SCLC behavior can be characterized by the Mott−Gurney square law, described as

$$J = (9/8)\varepsilon\mu(V^2/d^3)$$

where ε is the static dielectric constant of the medium (i.e., organic layer) and μ is the charge carrier mobility. The hole mobilities in the blends were estimated by fitting the $J-V$ curves with the SCLC model. The hole mobility (μ_h) of **P**−**F** blend film without additive, measured by the SCLC method, is 4.5×10^{-6} cm^2/(V·s), and it increases to 1.8×10^{-5} and 4.2×10^{-5} cm^2/(V·s) with DCB and CN additives, respectively. The hole mobility further increased up to 8.8×10^{-5} cm^2/(V·s) for the thermally annealed (CN additive) blend. Therefore, the hole mobility enhancement with the additive is caused by enhanced $\pi-\pi^*$ stacking and chain ordering, as supported by the UV and X-ray diffraction (XRD) data. We have also measured the electron mobility in the blend for an electron-only Al/**P**−**F**/Al device. The hole mobility increases by 1 order of magnitude, but the electron mobility (μ_e) remains almost the same. This observation shows that the **F** domain does not change much with the addition of additive in the solvent, resulting in similar electron mobility [2.8×10^{-4} cm^2/(V·s)]. With the hole mobility enhancement and a similar electron mobility, balanced holes and electrons could be achieved, which reduced the space charge resulting in the improved PCE of the device. The ratio μ_e/μ_h for the thermally annealed device cast from CN/THF solvent is 3.18, whereas this ratio is 62.2, 15.5, and 6.6 for devices cast from THF only, DCB/THF, and CN/THF, respectively. When the charge transport in the device is unbalanced (for example, device cast from THF only, where μ_h is significantly lower than μ_e), hole accumulation occurred in the device and the photocurrent was space-charge-limited.[44] However, the devices processed from mixed

Table 3. Calculated Data for P−F Blend Thin Films Cast from Different Solvents

parameters	THF (as cast)	DCB/THF (as cast)	CN/THF (as cast)	CN/THF (thermally annealed)
d spacing **P** (100) (Å)	14.56	14.61	14.65	14.72
crystallite size (nm)	10.4	12.6	14.2	16.3

solvents show higher hole mobility, due to the increased crystallite size of **P** in the blend, whereas the charge transport is more balanced and photocurrent is no more space-charge-limited, resulting in a higher value of PCE.

We have recorded the XRD profiles of **P** and **P**−**F** thin films cast from THF, DCB/THF, CN/THF (as cast), and CN/THF (thermally annealed) to investigate the change in crystallinity of the blends. Regardless of the solvent, all **P**−**F** films showed well-ordered **P** (100) (2θ = 8.28°) and (200) (2θ = 16.84°) peaks, which are related to the interchain of **P**. For **P**-only films, we observed the same (100) and (200) peaks, and these peaks have stronger intensity than those of the **P**−**F** film. This suggests that although the peak intensity of **P** is slightly reduced by blending **F** with **P**, copolymer **P** is well crystallized in all films prepared from different solvents. The films cast from CN/THF and CN/THF (thermally annealed) show stronger and sharper peaks than the one cast from DCB/THF solvent, indicating that the degree of **P** crystallization is better in the film cast from CN/THF solvent. In order to analyze the peaks in detail, XRD was performed with a narrow 2θ range (5−11°), in which only the **P** (100) peak is observed (Figure 10). The peak position corresponding to (100) is slightly shifted toward the low-angle side, indicating that the *d* spacing of **P** becomes larger during its crystallization. As can be seen from this figure, the slower evaporation (cast from mixed solvents) of the solvent leads to better crystallization, stronger interchain interaction, and well-defined crystallization peaks. From Figure 10, it was found that the **P**−**F** blend cast from CN/THF solvent had higher peak intensity and narrower half-width of (100) diffraction peak compared with films processed from the other solvents. The full width at maximum (B) of these (100) reflections gives an idea about the degree of crystallization and the crystallite size (d). We have calculated the *d* spacing parameter and crystallite size from the information of (100) peak using Bragg's and Scherrer's equation[45] (Table 3). The calculated grain size is related to the crystallite size along the normal to surface. It can be seen from Table 3 that both crystallite size and *d* spacing are increased for the mixed-solvent-cast films, which indicates that crystallization has been improved for the film cast from mixed solvents. The higher value of *d* spacing and crystallite size for the blend film cast from CN/THF solvent may be due to the higher value of boiling point of CN as compared to the DCB. The boiling point of a solvent is a critical parameter for inducing crystallinity of the blend. Higher boiling point solvents provide enough time for the blend crystallization process, which can facilitate highly crystalline growth.[46] Thermal annealing further improves the crystallization as observed from the XRD data [diffraction peak corresponds to (100) further intensify]. The increase in crystallite size also provides further insight into effective charge transport and also provides high internal effective field for charge separation, resulting in higher value of PCE.

CONCLUSIONS

A novel alternating phenylenevinylene copolymer, **P**, with thiophene and pyrrole rings was synthesized. It was soluble in common organic solvents and showed a broad absorption curve with long-wavelength absorption maximum at 596−635 nm and optical band gap of 1.65 eV, which is very close to the electrochemical band gap (1.70 eV) estimated by cyclic voltammetry. We have fabricated PSCs with the **P**−**F** blend and compared the photovoltaic performance with that of the device based on **P**−PCBM blend. The higher value of V_{oc} for devices based on **P** with respect to P3HT has been attributed to the deeper HOMO level of **P** as compared to P3HT. The PCE values of the devices based on **P**−PCBM and **P**−**F** processed from THF solvent are about 1.50% and 2.42%, respectively. The higher value of PCE for the device based on **P**−**F** blend is ascribed to the higher absorption coefficient of **F** in the visible region as compared to PCBM.

We have fabricated PSCs based on **P**−**F** blend processed from mixed solvents (DCB/THF and CN/THF) and found that the PCE values are 3.16% and 3.66%, respectively. The device based on **P**−**F** blend cast from CN/THF blend and subsequent thermal annealing shows a PCE of ∼4.14%. The increased PCE has resulted from the increased crystallite size of **P** in the blend, which in turn improves the hole mobility. The increase in hole mobility results in a more balanced charge transport in the device.

AUTHOR INFORMATION

Corresponding Author

*(J.A.M.) tel +30 2610 997115, fax +30 2610 997118, e-mail mikroyan@chemistry.upatras.gr; (G.D.S.) tel 91-0291-2720857, fax 91-0291-2720856, e-mail sharmagd_in@yahoo.com.

Present Addresses

§Solid State and Structural Chemistry Unit, Indian Institute of Science, Bangalore 560012, India.

REFERENCES

(1) Chen, M. H.; Hou, J.; Hong, Z.; Yang, G.; Sista, S.; Chen, L. M.; Yang, Y. *Adv. Mater.* **2009**, *21*, 1.

(2) Gadisa, A.; Oosterbaan, W. D.; Vandewal, K.; Bolsee, J. C.; Bertho, S.; Haen, J. D.; Lutsen, L.; Vanderzande, D.; Manca, J. V. *Adv. Funct. Mater.* **2009**, *19*, 1.

(3) Wang, E.; Wang, M.; Wang, L.; Duan, C.; Zhang, J.; Cai, W.; He, C.; Wu, H.; Cao, Y. *Macromolecules* **2009**, *42*, 4410.

(4) Wu, P. T.; Ren, G.; Kim, F. S.; Li, C.; Mezzenga, R.; Jenekhe, S. A. *J. Polym. Sci., Part A: Polym. Chem.* **2010**, *48*, 614.

(5) (a) Krebs, F. C.; Nielsen, T. D.; Fyenbo, J.; Wadstrom, M.; Pedersen, M. S. *Energy Environ. Sci.* **2010**, *3*, 512. (b) Krebs, F. C.; Fyenbo, J.; Jorgensen, M. *J. Mater. Chem.* **2010**, *20*, 8994. (c) Krebs, F. C.; Tromholt, T.; Jorgensen, M. *Nanoscale* **2010**, *2*, 873.

(6) (a) Brabec, C. J.; Sariciftci, N. S.; Hummelen, J. C. *Adv. Funct. Mater.* **2001**, *11*, 15. (b) Coakley, K. M.; McGehee, M. D. *Chem. Mater.* **2004**, *16*, 4533. (c) Spanggaard, H.; Krebs, F. C. *Sol. Energy Mater. Sol. Cells* **2004**, *83*, 125. (d) Hoppe, H.; Sariciftci, N. S. *J. Mater. Res.* **2004**, *19*, 1924. (e) Hoppe, H.; Sariciftci, N. S. *J. Mater. Chem.* **2006**, *16*, 45. (f) Günes, S.; Neugebauer, H.; Sariciftci, N. S. *Chem. Rev.* **2007**, *107*, 1324. (g) Thompson, B. C.; Fréchet, J. M. J. *Angew. Chem., Int. Ed.* **2008**, *47*, 58.

(7) Yu, G.; Gao, J.; Hummelen, J. C.; Wudl, F.; Heeger, A. J. *Science* **1995**, *270*, 1789.

(8) (a) Scharber, M. C.; Mühlbacher, D.; Koppe, M.; Denk, P.; Waldauf, C.; Heeger, A. J.; Brabec, C. J. *Adv. Mater.* **2006**, *18*, 789. (b) Bundgaard, E.; Krebs, F. C. *Macromolecules* **2006**, *39*, 2823. (c) Petersen, M. H.; Hagemann, O.; Nielsen, K. T.; Jørgensen, M.; Krebs, F. C. *Sol. Energy Mater. Sol. Cells* **2007**, *91*, 996. (d) Bundgaard, E.; Krebs, F. C. *Sol. Energy Mater. Sol. Cells* **2007**, *91*, 1019. (e) Bundgaard, E.; Shaheen, S. E.; Krebs, F. C.; Ginley, D. S. *Sol. Energy Mater. Sol. Cells* **2007**, *91*, 1631.

(9) Wienk, M. M.; Kroon, J. M.; Verhees, W. J. H.; Knol, J.; Hummelen, J. C.; van Hal, P. A.; Janssen, R. A. J. *Angew. Chem., Int. Ed.* **2003**, *42*, 3371.

(10) Shaheen, S. E.; Brabec, C. J.; Sariciftci, N. S.; Padinger, F.; Fromherz, T.; Hummelen, J. C. *Appl. Phys. Lett.* **2001**, *78*, 841.

(11) van Mullekom, H. A. M.; Vekemans, J. A. J. M.; Havinga, E. E.; Meijer, E. W. *Mater. Sci. Eng., R* **2001**, *32*, 1.

(12) (a) Brabec, C. J.; Winder, C.; Sariciftci, N. S.; Hummelen, J. C.; Dhanabalan, A.; van Hal, P. A.; Janssen, R. A. J. *Adv. Funct. Mater.* **2002**, *12*, 709. (b) Svensson, M.; Zhang, F. L.; Veenstra, S. C.; Verhees, W. J. H.; Hummelen, J. C.; Kroon, J. M.; Ingänas, O.; Andersson, M. R. *Adv. Mater.* **2003**, *15*, 988. (c) Zhou, Q. M.; Hou, Q.; Zheng, L. P.; Deng, X. Y.; Yu, G.; Cao, Y. *Appl. Phys. Lett.* **2004**, *84*, 1653. (d) Xia, Y. J.; Deng, X. Y.; Wang, L.; Li, X. Z.; Zhu, X. H.; Cao, Y. *Macromol. Rapid Commun.* **2006**, *27*, 1260. (e) Mühlbacher, D.; Scharber, M.; Morana, M.; Zhu, Z. G.; Waller, D.; Gaudiana, R.; Brabec, C. J. *Adv. Mater.* **2006**, *18*, 2884. (f) Hou, L. J.; He, C.; Han, M. F.; Zhou, E. J.; Li, Y. F. *J. Polym. Sci. Part A: Polym. Chem.* **2007**, *45*, 3861. (g) Blouin, N.; Michaud, A.; Leclerc, M. *Adv. Mater.* **2007**, *19*, 2295. (h) Zhu, Z. G.; Waller, D.; Gaudiana, R.; Morana, M.; Mühlbacher, D.; Scharber, M.; Brabec, C. J. *Macromolecules* **2007**, *40*, 1981. (i) Liao, L.; Dai, L. M.; Smith, A.; Durstock, M.; Lu, J. P.; Ding, J. F.; Tao, Y. *Macromolecules* **2007**, *40*, 9406.

(13) (a) Yang, R. Q.; Tian, R. Y.; Yan, J. G.; Zhang, Y.; Yang, J.; Hou, Q.; Yang, W.; Zhang, C.; Cao, Y. *Macromolecules* **2005**, *38*, 244. (b) Blouin, N.; Michaud, A.; Gendron, D.; Walkim, S.; Blair, E.; Neagu-Plesu, R.; Belletête, M.; Durocher, G.; Tao, Y.; Leclerc, M. *J. Am. Chem. Soc.* **2008**, *130*, 732.

(14) Zhan, X. W.; Tan, Z. A.; Domercq, B.; An, Z. S.; Zhang, X.; Barlow, S.; Li, Y. F.; Zhu, D. B.; Kippelen, B.; Marder, S. R. *J. Am. Chem. Soc.* **2007**, *129*, 7246.

(15) (a) Lee, S. K.; Cho, N. S.; Kwak, J. H.; Lim, K. S.; Shim, H. K.; Hwang, D. H.; Brabec, C. J. *Thin Solid Films* **2006**, *511*, 157. (b) Thompson, B. C.; Kim, Y. G.; McCarley, T. D.; Reynolds, J. R. *J. Am. Chem. Soc.* **2006**, *128*, 12714. (c) Colladet, K.; Fourier, S.; Cleij, T. J.; Lutsen, L.; Gelan, J.; Vanderzande, D.; Nguyen, L. H.; Neugebauer, H.; Sariciftci, S.; Aguirre, A.; Janssen, G.; Goovaerts, E. *Macromolecules* **2007**, *40*, 65.

(16) (a) Shaheen, S. E.; Vangeneugden, D.; Kiebooms, R.; Vanderzande, D.; Fromherz, T.; Padinger, F.; Brabec, C. J.; Sariciftci, N. S. *Synth. Met.* **2001**, *121*, 1583. (b) Wang, X. J.; Perzon, E.; Delgado, J. L.; De la Cruz, P.; Zhang, F. L.; Langa, F.; Andersson, M.; Ingänas, O. *Appl. Phys. Lett.* **2004**, *85*, 5081. (c) Zhang, F. L.; Perzon, E.; Wang, X. J.; Mammo, W.; Andersson, M. R.; Ingänas, O. *Adv. Funct. Mater.* **2005**, *15*, 745. (d) Campos, L. M.; Tontcheva, A.; Günes, S.; Sonmez, G.; Neugebauer, H.; Sariciftci, N. S.; Wudl, F. *Chem. Mater.* **2005**, *17*, 4031. (e) Zhang, F. L.; Mammo, W.; Andersson, L. M.; Admassie, S.; Andersson, M. R.; Ingänas, O. *Adv. Mater.* **2006**, *18*, 2169. (f) Wienk, M. M.; Turbiez, M. G. R.; Struijk, M. P.; Fonrodona, M.; Janssen, R. A. J. *Appl. Phys. Lett.* **2006**, *88*, No. 153511.

(17) (a) Huo, L.; Hou, J.; Zhang, S.; Chen, H. Y.; Yang, Y. *Angew. Chem.* **2010**, *49*, 1500. (b) Hou, J.; Chen, H. Y.; Zhang, S.; Li, G.; Yang, Y. *J. Am. Chem. Soc.* **2008**, *130*, 16144. (c) Zou, Y.; Naiari, A.; Berrouard, P.; Beaupre, S.; Aich, B. R.; Tao, Y.; Leclerc, M. *J. Am. Chem. Soc.* **2010**, *132*, 5330. (d) Liang, Y.; Wu, Y.; Feng, D.; Tsai, S. T.; Son, H. J.; Li, G.; Yu, L. *J. Am. Chem. Soc.* **2009**, *131*, 56. (e) Qin, R.; Li, W.; Li, C.; Du, C.; Veit, C.; Schleiermacher, H. F.; Adersson, M.; Bo, Z.; Liu, Z.; Inganas, O.; Wuerfel, U.; Zhang, F. *J. Am. Chem. Soc.* **2009**, *131*, 14612. (f) Chen, H. Y.; Hou, J.; Zhang, S.; Liang, Y.; Yang, G.; Yu, I.; Wu, Y.; Li, G. *Nat. Photon* **2009**, *3*, 649. (g) Park, S. H.; Roy, A.; Beaupre, S.; Cho, S.; Coates, N.; Moon, J. S.; Moses, D.; Leclerc, M.; Lee, K.; Heeger, A. J. *Nat. Photon* **2009**, *3*, 297. (h) Linag, Y.; Xu, Z.; Xia, J.; Tsai, S. T.; Wu, Y.; Li, G.; Ray, C.; Yu, L. *Adv. Mater.* **2010**, *22*, E135. (i) Wang, E.; Wang, L.; Lan, L.; Luo, C.; Zhang, W.; Peng, J.; Cao, Y. *Appl. Phys. Lett.* **2008**, *92*, No. 033307. (j) Muhlbacher, D.; Scharber, M.; Morana, M.; Zhu, Z. G.; Waller, D.; Gaudiana, R.; Brabec, C. *Adv. Mater.* **2006**, *18*, 2884.

(18) (a) www.solarmer.com. (b) www.konarka.com.

(19) (a) van Haare, J. A. E. H.; Groenendaal, L.; Peerlings, H. W. I.; Havinga, E. E.; Vekemans, J. A. J. M.; Janssen, R. A. J.; Meijer, E. W. *Chem. Mater.* **1995**, *7*, 1984. (b) van Haare, J. A. E. H.; Groenendaal, L; Havinga, E. E.; Janssen, R. A. J.; Meijer, E. W. *Angew. Chem.* **1996**, *108*, 696.

(20) (a) Yu, M.; Pantos, G. D.; Sessler, J. S.; Pagenkopf, B. L. *Org. Lett.* **2004**, *6*, 1057. (b) Pappenfus, T. M.; Hermanson, B. J.; Helland, T. J.; Lee, G. G. W.; Drew, S. M.; Mann, K. R.; McGee, K. A.; Rasmussen, S. C. *Org. Lett.* **2008**, *10*, 1553.

(21) (a) Sessler, J. L.; Aguilar, A.; Sanchez-Garcia, D.; Seidel, D.; Kohler, T.; Arp, F.; Lynch, V. M. *Org. Lett.* **2005**, *7*, 1887. (b) Fujii, M.; Nishinaga, T.; Iyoda, M. *Tetrahedron Lett.* **2009**, *50*, 555.

(22) Tamilavan, V.; Song, M.; Jin, S.-H; Hyun, M. H. *J. Polym. Sci., Part A: Polym. Chem.* **2010**, *48*, 5514.

(23) Yue, W.; Zhao, Y.; Shao, S.; Tian, H.; Xie, Z.; Geng, Y.; Wang, F. *J. Mater. Chem.* **2009**, *19*, 2199.

(24) Zhang, X.; Steckler, T. T.; Dasari, R. R.; Ohira, S.; Potscavage, W. J., Jr.; Tiwari, S. P.; Coppee, S.; Ellinger, S.; Barlow, S.; Bredas, J.-L.; Kippelen, B.; Reynolds, J. R.; Marder, S. R. *J. Mater. Chem.* **2010**, *20*, 123.

(25) Price, S. C.; Stuart, A. C.; You, W. *Macromolecules* **2010**, *43*, 797.

(26) Dhanabalan, A.; Van Duren, J. K. J.; Van Hal, P. A.; Van Dongen, J. L. J.; Janssen, R. A. J. *Adv. Funct. Mater.* **2001**, *11*, 255.

(27) Liu, Y.; Summers, M. A.; Edder, C.; Frechet, J. M. J.; McGehee, M. D. *Adv. Mater.* **2005**, *17*, 2960.

(28) Tamilavan, V.; Sakthivel, P.; Li, Y.; Song, M.; Kim, C. H.; Jin, S. H.; Hyun, M. H. *J. Polym. Sci., Part A: Polym. Chem.* **2010**, *48*, 3169.

(29) Mikroyannidis, J. A.; Kabanakis, A. N.; Balraju, P.; Sharma, G. D. *Macromolecules* **2010**, *43*, 5544.

(30) Mikroyannidis, J. A.; Kabanakis, A. N.; Sharma, S. S.; Sharma, G. D. *Adv. Funct. Mater.* **2011**, *21*, 746.

(31) Robertson, G. R. *Organic Syntheses*; Wiley: New York, 1941; Collect. Vol. 1, p 396 [*Org. Synth.* 1922, 2, 57].

(32) Liu, X.; Zhou, X.; Shu, X.; Zhu, J. *Macromolecules* **2009**, *42*, 7634.

(33) McKean, D. R.; Parrinello, G.; Renaldo, A. F.; Stille, J. K. *J. Org. Chem.* **1987**, *52*, 422.

(34) Peng, Q.; Li, M.; Tang, X.; Lu, S.; Peng, J.; Cao, Y. *J. Polym. Sci., Part A: Polym. Chem.* **2007**, *45*, 1632.

(35) Kenning, D.; Mitchell, K. A.; Calhoun, T. R.; Funfar, M. R.; Sattler, D. J.; Rasmussen, S. C. *J. Org. Chem.* **2002**, *67*, 9073.

(36) (a) Li, Y.; Cao, Y.; Gao, J.; Wang, D.; Yu, G.; Heeger, A. J. *Synth. Met.* **1999**, *99*, 243. (b) Sun, Q. J.; Wang, H. Q.; Yang, C. H.; Li, Y. F. *J. Mater. Chem.* **2003**, *13*, 800.

(37) (a) Thompson, B. C.; Kim, Y. G.; Reynolds, J. R. *Macromolecules* **2005**, *38*, 5359. (b) de Leeuw, D. M.; Simenon, M. M. J.; Brown, A. R.; Einerhand, R. E. F. *Synth. Met.* **1997**, *87*, 53.

(38) Thompson, B. C.; Frechet, J. M. J. *Angew. Chem., Int. Ed.* **2008**, *47*, 58.

(39) Zhu, Y.; Champion, R. D.; Jeneke, S. A. *Macromolecules* **2006**, *39*, 871.

(40) Zoombelt, A. P.; Fonrodona, M.; Turbiez, M. G. R.; Wienk, M. M.; Janssen, R. A. J. *J. Mater. Chem.* **2009**, *19*, 5336.

(41) He, Y.; Chen, H. Y.; Hou, J.; Li, Y. *J. Am. Chem. Soc.* **2010**, *132*, 1377.

(42) (a) Peet, J.; Kim, J. Y.; Coates, N. E.; Ma, W. L.; Moses, D.; Heeger, A. J.; Bazan, G. C. *Nat. Mater.* **2005**, *6*, 497. (b) Peet, J.; Senatore, M. L.; Heeger, A. J.; Bazan, G. C. *Adv. Funct. Mater.* **2009**, *21*, 1521. (c) Woo, C. H.; Beaujuge, P. M.; Holcombe, T. W.; Lee, O. P.; Frechet, J. M. J. *J. Am. Chem. Soc.* **2010**, *132*, 15547. (d) Lee, J. K.; Ma, W. L.; Brabec, C. J.; Yuen, J.; Moon, J. S.; Kim, J. Y.; Lee, K.; Bazan, G. C. *J. Am. Chem. Soc.* **2008**, *130*, 3619. (e) Kim, J. H.; Park, J. H. Lee, J. H.; Kim, J. S.; Sim, M.; Shim, C.; Cho, K. *J. Mater. Chem.* **2010**, *20*, 7398. (f) Chan, S. H.; Hsiao, Y. S.; Hung, L. I.; Hwang, G. W.; Chen,

H. L.; Ting, C.; Chen, C. P. *Macromolecules* **2010**, *43*, 3399. (g) Moon, J. S.; Takacs, C. J.; Cho, S.; Coffin, R. C.; Kim, H.; Bazan, G. C.; Heeger, A. J. *Nano Lett.* **2010**, *10*, 4005–4008.

(43) (a) Lampert, M. A.; Mark, P. *Current Injection in Solids*; Academic Press: New York, 1970. (b) Mihaitetchi, V. D.; Xie, H.; de Boer, B.; Koster, L. J. A.; Blom, P. W. M. *Adv. Funct. Mater.* **2006**, *16*, 699. (c) Zhao, Y.; Xie, Z.; Qu, Y.; Geng, Y.; Wang, L. *Appl. Phys. Lett.* **2007**, *90*, No. 043504.

(44) Moule, A. J.; Meerholz, K. *Adv. Mater.* **2008**, *20*, 240.

(45) Cullity, B. D.; Stock, S. R. *Elements of X-ray Diffraction*, 3rd ed.; Prentice Hall Inc.: Upper Saddle River, NJ, 2001; p 167.

(46) (a) Li, G.; Yao, Y.; Yang, H.; Shrotriya, V.; Yang, G. *Adv. Funct. Mater.* **2007**, *17*, 1636. (b) Cheng, H. L.; Lin, W. Q.; Wu, F. C. *Appl. Phys. Lett.* **2009**, *94*, No. 223302.